

# Boehmite-supported CuO as a catalyst for catalytic transfer hydrogenation of 5-hydroxymethylfurfural to 2,5-bis(hydroxymethyl)furan

Zexing Huang<sup>1</sup>, Zhijuan Zeng<sup>1</sup>, Xiaoting Zhu<sup>1</sup>, Wenguang Zhao<sup>1</sup>, Jing Lei<sup>2</sup>,  
Qiong Xu<sup>1</sup>, Yongjun Yang<sup>2</sup>, Xianxiang Liu (✉)<sup>1</sup>

1 National & Local Joint Engineering Laboratory for New Petro-chemical Materials and Fine Utilization of Resources, Key Laboratory of the Assembly and Application of Organic Functional Molecules of Hunan Province, Hunan Normal University, Changsha 410081, China

2 Chenzhou Gao Xin Material Co., Ltd., Chenzhou 423000, China

© Higher Education Press 2022

**Abstract** 2,5-bis(hydroxymethyl)furan (BHMF) is an important monomer of polyester. Its oxygen-containing rigid ring structure and symmetrical diol functional group establish it as an alternative to petroleum-based monomer with unique advantages for the production of the degradable bio-based polyester materials. Herein, we prepared a boehmite-supported copper-oxide catalyst for the selective hydrogenation of 5-hydroxymethylfurfural into BHMF via catalytic transfer hydrogenation (CTH). Further, ethanol successfully replaced conventional high-pressure hydrogen as the hydrogen donor, with up to 96.9% BHMF selectivity achieved under suitable conditions. Through characterization and factor investigations, it was noted that CuO is crucial for high BHMF selectivity. Furthermore, kinetic studies revealed a higher by-product activation energy compared to that of BHMF, which explained the influence of reaction temperature on product distribution. To establish the catalyst structure-activity correlation, a possible mechanism was proposed. The copper-oxide catalyst deactivated following CTH because ethanol reduced the CuO, which consequently decreased the active sites. Finally, calcination of the catalyst in air recovered its activity. These results will have a positive impact on hydrogenation processes in the biomass industry.

**Keywords** biomass, 5-hydroxymethylfurfural, 2,5-bis(hydroxymethyl)furan, transfer hydrogenation, catalysis

## 1 Introduction

Improving chemical reaction selectivity is of significant

Received March 29, 2022; accepted July 26, 2022

E-mail: lxx@hunnu.edu.cn

importance in various industries and applications. Furthermore, selective hydrogenation has been widely investigated in previous decades because of its ability to reduce unsaturated groups in various compounds, such as C=C, C=O, C≡C, C≡N, and aromatic ring containing compounds. The development of methods to ensure high selectivity for target functional group reductions is essential from a commercial viewpoint, as it can yield various value-added chemicals and broaden current chemical knowledge.

5-hydroxymethylfurfural (HMF), which is an important biomass platform, is a major focus of biomass research. Several high-value chemicals can be produced from HMF reduction, such as 5-methylfurfural, 2,5-bis(hydroxymethyl)furan (BHMF), 2,5-dimethyltetrahydrofuran, and 2,5-dimethylfuran [1,2]. BHMF is a key monomer employed for the synthesis of foam, polyether, and crown ethers owing to its oxygen-containing rigid ring structure and symmetrical diol functional group, which provide unique advantages over conventional polyester industry chemicals [3–5]. However, selectively reducing the furan ring aldehyde group during HMF to BHMF conversion remains challenging. Hydrogenation processes primarily use high-pressure hydrogen as a hydrogen donor because of its low solubility in organic solutions, resulting in a high BHMF yield at relatively mild reaction temperatures [5]. Recently, Rao et al. [6] prepared a Cu/Al<sub>2</sub>O<sub>3</sub> catalyst for the selective hydrogenation of HMF using solvent-free solid-state grinding, achieving a 92% yield under a 3 MPa hydrogen atmosphere. When Co/C was used as the catalyst, BHMF was synthesized over 6 h at a yield of 93% under a 2 MPa hydrogen atmosphere [7]. Zhao et al. [8] prepared a nickel–cobalt bimetallic catalyst for HMF hydrogenation, obtaining a BHMF yield of 93.1% under a 0.5 MPa hydrogen atmosphere at 373 K. Thus, there has

been significant progress regarding BHMF synthesis in a hydrogen atmosphere. However, several drawbacks are associated with hydrogen use as hydrogen is difficult to transport and store, and it poses a considerable safety risk because of its inflammability [4]. Additionally, hydrogen use violates the requirements of clean biomass energy development, as hydrogen is primarily obtained by fossil fuel cracking. In contrast to hydrogen, formic acid and alcohols, such as methanol and ethanol, are liquid at room temperature and pressure, prompting their use as external hydrogen substitutes in recent years. Although formic acid has exhibited excellent performance as a hydrogen donor for the catalytic transfer hydrogenation (CTH) of HMF, its applicability was limited when metal catalysts such as Pd/C and Ni–Co/C were used because of its propensity to corrosion. This can poison the catalyst, thereby adversely affecting its reusability, and acidity enable formic acid to react with BHMF forming esterification by-product [9,10].

Alcohols are highly promising hydrogen donors for HMF hydrogenation via the Meerwein–Ponndorf–Verley (MPV) reduction method as they are inexpensive and safer than molecular hydrogen [11–13]. Wang et al. [11] used mesoporous carbon-supported Co nanoparticles as a catalyst with unsaturated aldehydes for CTH and achieved a 97% BHMF yield over 48 h. Hu et al. [12] prepared an acid-base bifunctional Zr-containing organic–inorganic nanohybrid catalyst, which resulted in a 95% BHMF yield over 4 h at 413 K. Thus, designing a suitable catalyst for the selective hydrogenation of HMF to BHMF via the MPV reaction is necessary. Of the aforementioned catalysts, the metallic catalysts consisting of a two-metal/substrate support exhibit better catalytic activity than the monometallic catalysts. This favorable performance is attributed to the synergetic effects of the geometric and electronic interactions between the two metals [14–16]. Elsayed et al. [14] reported a bimetallic nanocatalyst supported on activated carbon ( $\text{CuO}-\text{Fe}_3\text{O}_4$ /activated carbon) for the selective hydrogenation of HMF to BHMF using ethanol as the hydrogen donor; a 94% yield was achieved at 413 K over 5 h. Wang et al. [15] synthesized a Ru/ $\text{Co}_3\text{O}_4$  catalyst and tested it for the CTH of HMF to BHMF using isopropanol as the hydrogen donor, achieving an 82% diol yield at 463 K. Zhang et al. [16] designed a carbon-nanosheet-supported Zr/Ca bimetallic catalyst that was used for the CTH of HMF to BHMF, and achieved an 84% BHMF yield at 463 K over 10 h. Thus, non-noble metal catalysts have been widely investigated for the hydrogenation of HMF to BHMF. Al is an inexpensive representative metal as its oxide exhibits increased activity in the CTH reaction owing to the large number of Lewis acid sites present on its surface. However, the high adsorption capacity of  $\text{Al}_2\text{O}_3$  results in a low substrate conversion rate, as well as a subsequent hydroxyl reaction. Huang et al. [18] inhibited these undesirable outcomes by modifying  $\text{Al}_2\text{O}_3$  using Cu.

Herein, to accomplish transfer hydrogenation via the MPV method, while also exploiting the advantages of metal catalysts for surface modification, the selective hydrogenation of HMF to BHMF over catalyst samples was performed. The catalysts consisted of CuO in different amounts supported on boehmite (Bhm), a form of  $\text{AlO}(\text{OH})$ . The catalysts were prepared using the precipitation–deposition method and characterized with respect to factors affecting the hydrogenation process, i.e., reaction time, catalyst loading, and temperature optimized to maximize the BHMF yield.

## 2 Experimental

### 2.1 Materials

HMF ( $\geq 98.0\%$ ) was purchased from Shanghai D&B Biological Science and Technology Co., Ltd. (Shanghai, China). BHMF (98.0%) was purchased from Energy Chemical Co., Ltd. (Shanghai, China). Bhm (AR grade),  $\text{Cu}(\text{NO}_3)_2 \cdot 3\text{H}_2\text{O}$  (AR grade), ethanol (AR grade), and octane (CP grade) were purchased from Sinopharm Chemical Reagent Co., Ltd. (Shanghai, China). NaOH was purchased from Tianjin HengXing Chemical Reagent Co., Ltd. (Tianjin, China).

### 2.2 Catalyst preparation

The catalyst samples were synthesized using the conventional deposition–precipitation method. Based on the target weight ratio ( $\text{CuO:Bhm} = 2:3$ ),  $\text{Cu}(\text{NO}_3)_2 \cdot 3\text{H}_2\text{O}$  (2 g) was measured and placed in a beaker. Ultrapure water (100 mL) was then added under continuous stirring for 5 min. Next, Bhm (2 g) was added to the  $\text{Cu}(\text{NO}_3)_2$  solution to form a suspension, followed by adjusting the suspension pH to 8 using a NaOH solution. This mixture was then stirred for 4 h at 333 K and then allowed to age for 1 h. Finally, a dark blue solid (precursor) was obtained following filtration, which was subsequently dried at 393 K for 12 h. Next, the precursor was calcined in a tubular furnace at 673 K for 2 h at a flow rate of  $100 \text{ mL} \cdot \text{min}^{-1}$  under a nitrogen atmosphere. A heating rate of  $5 \text{ K} \cdot \text{min}^{-1}$  from 323 to 673 K was observed. The prepared catalyst sample was labeled as  $x$  wt % CuO/Bhm (with  $x$  wt % being the amount of CuO added) for convenience.

### 2.3 Catalyst characterization

The X-ray diffraction (XRD) patterns of the catalyst samples were recorded using an Ultima IV powder X-Ray diffractometer (Rigaku, Japan) with a Cu- $\text{K}\alpha$  radiation source with a tube pressure of 40 kV for the diffraction angle ( $2\theta$ ) ranging from  $10^\circ$ – $90^\circ$ . X-ray photoelectron spectroscopy (XPS) was performed using a K-Alpha spectrometer (Thermo Scientific, USA) under vacuum,

and the profiles were corrected based on the C 1s line at 284.80 eV. Nitrogen adsorption measurements were performed on the catalyst samples using an ASAP 2460 sorption analyzer (Micromeritics, USA). The samples were outgassed at 473 K for 4 h before the measurements. NH<sub>3</sub>-temperature-programmed desorption (TPD) measurements were performed to measure the acidity using an AMI-300 instrument (Altamira, USA) connected to a thermal conductivity detector.

#### 2.4 Catalytic activity test

HMF (1 mmol, 126 mg), the catalyst sample (100 mg), and ethanol (10.0 mL) were added to a 50-mL autoclave with a Teflon liner, which was subsequently sealed and purged with N<sub>2</sub> four times before filling with N<sub>2</sub> at 0.1 MPa. The HMF hydrogenation was performed at a controlled temperature and pressure under stirring. Following reaction completion, the reactor was cooled in ice water and the liquid products were analyzed using gas chromatography (GC) (Nexis GC-2030, Shimadzu, Japan) with a flame ionization detector and a capillary column (SH-Rtx-1701). The structural characteristics of the samples were analyzed further by GC-mass spectrometry (Fig. S1, cf. Electronic Supplementary Material, ESM). The parameters used for the GC measurements were as follows: The injection volume and split ratio were 1.0 μL and 1:40. The temperatures of the injection port and the detector were both 723 K. The temperature program used was as follows: 313 K for 3 min, 313–373 K (10 K·min<sup>-1</sup>), 373 K for 1 min, 373–473 K (40 K·min<sup>-1</sup>), and 473 K for 2 min.

### 3 Results and discussion

#### 3.1 Catalyst characterization

The XRD patterns of the CuO/Bhm catalyst samples with different CuO concentrations are shown in Fig. 1. The analyzed samples exhibited peaks characteristic of Bhm and the monoclinic crystal structure of CuO. This confirmed that the Bhm structure remained intact throughout the catalyst synthesis process. Additionally, diffraction peaks related to the (020), (120), (031), and (131) lattice planes of γ-AlO(OH) were observed at 2θ values of 14.5°, 28.2°, 38.3°, and 45.8° in the patterns of all the samples (International Centre for Diffraction Data (ICDD) No. 21-1307), respectively. The diffraction peaks at the 2θ of 32.5°, 35.4°, 38.7°, and 38.9° could be assigned to the (110), (002), (111), and (200) reflections of CuO (ICDD No. 48-1548), respectively. The CuO phase peak presence indicated that the deposition–precipitation method resulted in sufficient loading of the metal oxide onto the Bhm surface. Noticeably, the peak

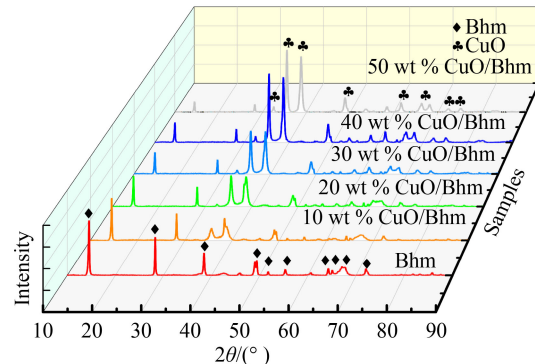


**Fig. 1** XRD patterns of the synthesized CuO/Bhm catalyst samples.

intensities related to the CuO phase increased as the CuO content in the catalyst increased to 40 wt %.

The Brunauer–Emmett–Teller (BET) and Barrett–Joyner–Halenda methods examined the physical characteristics of the samples, i.e., their pore volume, pore size, and surface area (see Table 1). The Bhm possessed the largest BET surface area (130.68 m<sup>2</sup>·g<sup>-1</sup>) and the smallest average pore diameter (4.98 nm). After coating the Bhm with CuO, the surface areas of the resultant catalyst samples gradually decreased with an increase in the CuO loading quantity. All of the prepared samples were mesoporous, with a wide distribution of enlarged pores. The reduction in surface area can be attributed to metal oxide deposition on the Bhm surface that occurred during the calcination step of the catalyst synthesis. The N<sub>2</sub> adsorption–desorption isotherms and pore size distribution–desorption isotherms of the different catalyst samples are shown in Fig. 2. A typical type-IV isotherm with a hysteresis loop of type H1 was observed for the Bhm and 40 wt % CuO/Bhm, strongly indicating the presence of a mesoporous catalyst structure. Figure 3 displays the NH<sub>3</sub>-TPD profiles of the Bhm and 40 wt % CuO/Bhm. Both exhibit an obvious peak related to NH<sub>3</sub> desorption at 420 K, which was caused by the AlO(OH) acid sites. Additionally, the 40 wt % CuO/Bhm shows a significant NH<sub>3</sub> desorption peak at 530 K, suggesting that a stronger acidity is associated with the 40 wt % CuO/Bhm than with the Bhm. The number of acid sites on the 40 wt % CuO/Bhm was highest at 665.89 μmol·g<sup>-1</sup>,

**Table 1** Main physicochemical properties of the CuO/Bhm catalysts

Sample	BET / (m <sup>2</sup> ·g <sup>-1</sup> )	V <sub>pore</sub> / (cm <sup>3</sup> ·g <sup>-1</sup> )	D <sub>pore</sub> / nm	Amount of acid sites / (μmol·g <sup>-1</sup> ) <sup>a</sup>
Bhm	130.68	0.19	4.98	472.15
10 wt % CuO/Bhm	116.53	0.26	7.71	344.98
20 wt % CuO/Bhm	105.94	0.26	8.30	506.65
30 wt % CuO/Bhm	94.65	0.30	10.79	263.95
40 wt % CuO/Bhm	80.66	0.17	7.35	665.89
50 wt % CuO/Bhm	65.89	0.16	8.24	459.13

<sup>a</sup>) The amount of acid sites represents the total number of acid sites on the catalyst surface.

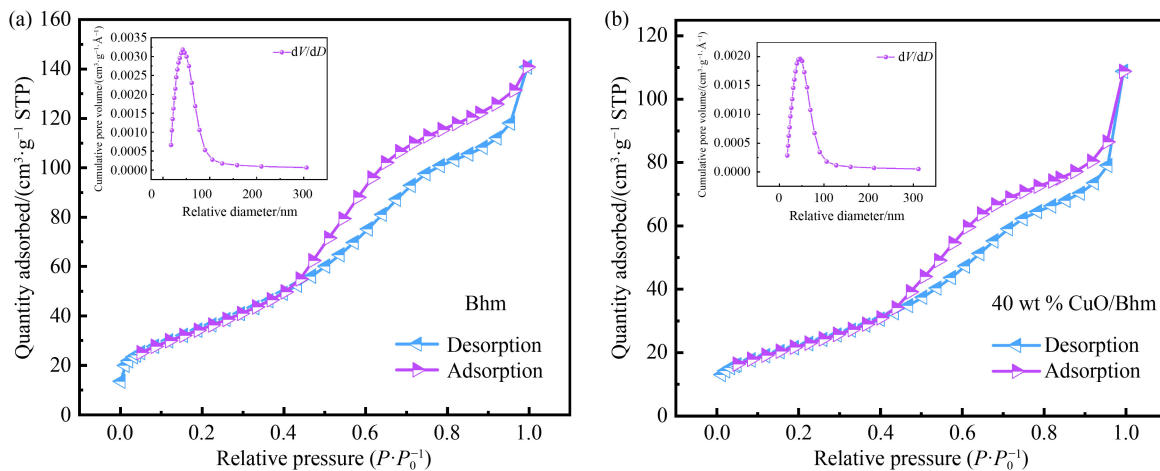


**Fig. 2**  $\text{N}_2$  adsorption–desorption isotherms and pore size distribution curves of (a) Bhm and (b) 40 wt % CuO/Bhm.

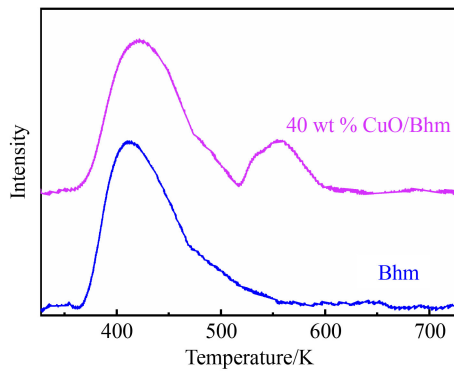


**Fig. 3**  $\text{NH}_3$ -TPD profiles of Bhm and 40 wt % CuO/Bhm.

which was 1.4 times greater than that of the Bhm (Table 1). Further, the concentration of loaded CuO influenced the number of acid sites and the BHMF selectivity; however, the total number of acid sites did not directly dictate BHMF selectivity.

The XPS profiles of the catalysts are shown in Fig. 4. Corrections were performed using the C 1s line at 284.80 eV (Fig. 4(a)). The binding energy peak at 75.69 eV is generally associated with the Al of  $\text{Al}(\text{OH})_3$  [19]. From the XPS profile, only CuO exhibited binding energy peaks at 933.46 and 953.58 eV, which correspond to  $\text{Cu}^{2+}$  2p3/2 and  $\text{Cu}^{2+}$  2p1/2, respectively [20]. The binding energy peak at 935.08 eV, which was absent from the pure CuO sample, represents the Bhm species. Majid et al. [21] reported similar phenomena whereby the pure CuO sample had a singular  $\text{Cu}^{2+}$  2p3/2 signal at 933.8 eV, but  $\text{SnO}_2/\text{CuO}$  had two signals at 934.2 and 932.6 eV, respectively. The binding energies for the O 1s lines of CuO and the hydroxyl group were 529.48 and 531.15 eV, respectively [19,20]. This result can be attributed to CuO present on the Bhm surface. Furthermore, the hydroxyl groups were abundantly distributed on the Bhm surface, while the  $\text{H}^+$  ions (Brønsted acids) catalyzed the alcohol etherification [22]. The  $\text{Cu}^{2+}$  (Lewis acid) presence proportionally decreased the number of Brønsted acid

sites, which reduced the yield of 2-hydroxymethyl-5-ethoxyfuran (HEMF, Fig. S2, cf. ESM). Therefore, the BHMF selectivity increased when CuO-modified Bhm was used as the catalyst.

### 3.2 Catalytic CTH reaction of HMF to BHMF

The blank experiment result indicates that HMF transformed into unknown products in the absence of a catalyst (Fig. S3, cf. ESM). Contrastingly, CuO exhibited very low catalytic activity while HMF did not react with the other substances. Several by-products, including HEMF, were detected when Bhm catalyzed the CTH reaction of HMF to BHMF (Table 2). Reduced Bhm resulted in greater HEMF production owing to the presence of the oxygen vacancies, which increased the acidity and catalyzed the etherification reaction; these results corroborate with those of a previous study [23]. To inhibit the Bhm etherification catalytic activity, 10 wt % CuO was added to the Bhm surface to synthesize 10 wt % CuO/Bhm. The BHMF selectivity significantly improved from 59.7% to 87.8%, while the HMF conversion rate slightly decreased. This suggested the importance of Bhm in the CTH reaction, and that the presence of CuO inhibited the BHMF etherification reaction. Furthermore, the addition of CuO hindered the hydroxyl  $\text{H}^+$  (Brønsted acid sites) from catalyzing the BHMF reaction with ethanol. To further elucidate the effects of the CuO concentration present on the Bhm surface, 10–50 wt % CuO/Bhm samples were synthesized and used for the CTH conversion of HMF into BHMF. Noticeably, the BHMF selectivity reached 96.9% at a CuO content of 40% (Table 2). Additionally, CuO and Bhm were also mechanically mixed, and the mixture was used to catalyze HMF CTH, resulting in a BHMF selectivity of 86%. Thus, it was confirmed that the CuO presence on the Bhm surface influenced catalytic activity, and that controlled CuO use is pivotal to ensure high BHMF selectivity. Contrastingly, 50 wt % CuO/Bhm did not efficiently

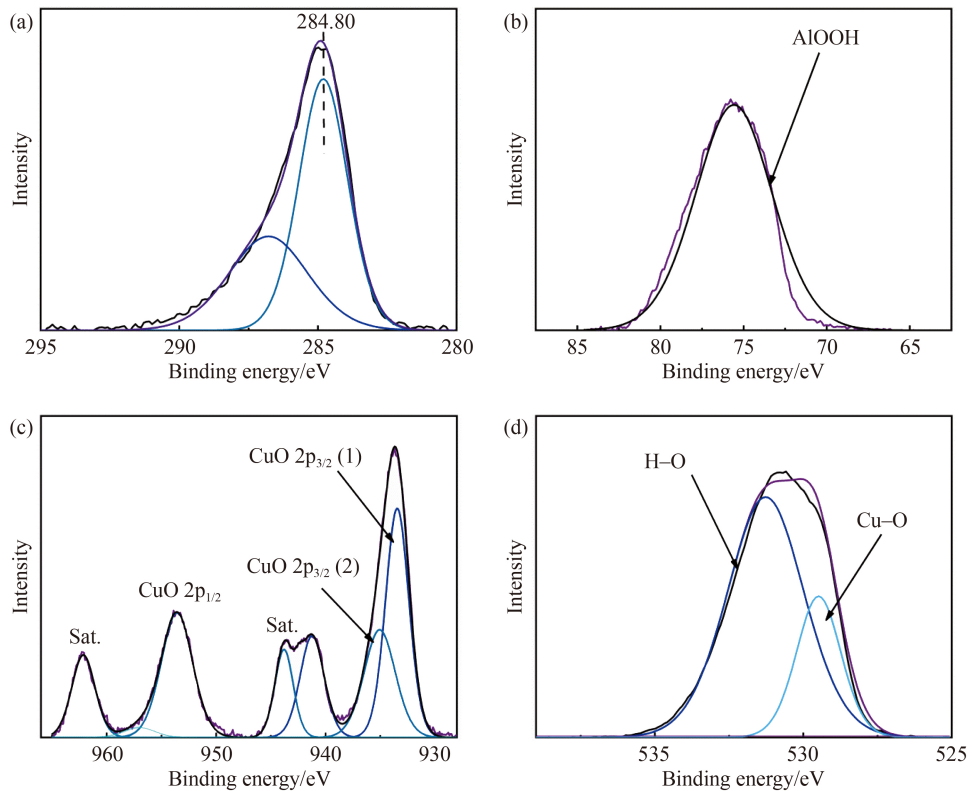


**Fig. 4** XPS profiles of 40 wt % CuO/Bhm. (a) C 1s; (b) Al 2p; (c) Cu 2p; (d) O 1s.

**Table 2** Effect of different catalyst samples on BHMF selectivity and HMF conversion <sup>a)</sup>

Entry	Catalyst	HMF conversion/%	Selectivity/%		
			BHMF	HEMF	Others
1	Blank	36.2	0	0	100
2	CuO	9.9	88.1	7.9	4.0
3	Bhm	72.1	59.7	25.1	15.2
4	Bhm <sup>b)</sup>	79.6	45.5	39.4	17.1
5	10 wt % CuO/Bhm	72.7	87.8	11.7	1.5
6	20 wt % CuO/Bhm	71.6	91.2	6.6	2.2
7	30 wt % CuO/Bhm	72.5	90.7	7.3	2.0
8	40 wt % CuO/Bhm	75.9	96.9	3.6	0.5
9	40 wt % CuO/Bhm <sup>c)</sup>	37.2	86.7	7.2	5.9
10	50 wt % CuO/Bhm	38.5	0	0	100

a) Reaction conditions: 10 mL ethanol, 1 mmol HMF, catalyst/HMF = 80%, time = 3 h, temperature = 433 K; b) Bhm was reduced to generate oxygen vacancies; c) CuO and Bhm were mechanically mixed.

catalyze HMF into BHMF. It even produced an unknown compound (Fig. S4, cf. ESM), which formed a bright yellow reaction solution (Fig. S5, cf. ESM). Thus, 40 wt % CuO/Bhm was considered the optimal catalyst and used for subsequent experiments.

The type of hydrogen donor solvent significantly influenced the CTH of HMF to BHMF. Here, different hydrogen donor alcohols were tested to determine the species with the highest affinity for the hydrogenation reaction (Fig. 5). Increasing the molecular weight of the alcohols decreased their hydrogen donation abilities,

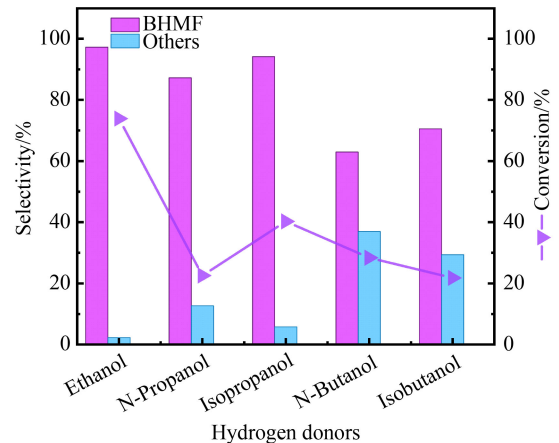


**Fig. 5** Effect of the hydrogen donor reaction (reaction conditions: 10 mL hydrogen donor, 1 mmol HMF, catalyst/HMF = 80%, time = 3 h, temperature = 433 K).

possibly owing to steric hindrance. Interestingly, the secondary alcohols exhibited higher BHMF selectivity than the corresponding primary alcohols, potentially because of the increased stability of the carbocations formed from the secondary alcohols than their corresponding primary alcohols [24]. This is likely because of an initial BHMF carbocation formation that conjugates with the furan ring and subsequently reacts with the alcohol to form by-products. Following testing, ethanol was chosen as the hydrogen donor for subsequent experiments because of its favorable performance.

Performing the HMF hydrogenation reaction at elevated temperatures resulted in a higher BHMF yield, as well as more unwanted by-products (see Fig. 6). The BHMF selectivity and HMF conversion rate were studied at comparatively lower temperatures (413–453 K). HMF was unreacted with ethanol at 413 K; however, increasing the reaction temperature to 433 K had a noticeable effect on the HMF conversion rate, which increased from 5.6% to 75.9%, while also slightly decreasing the BHMF selectivity. A temperature increase to 453 K slightly improved the HMF conversion rate. However, this coincided with a sharp increase in the by-product formation. Therefore, 433 K was chosen as the optimal reaction temperature for the HMF to BHMF hydrogenation.

Figure 7 shows that the catalyst dosage also affected the CTH of HMF to BHMF. The BHMF selectivity was lowest using a catalyst/HMF ratio of 20%. An increase to 60% consequently increased the selectivity to 97.3%. This is because increasing the ratio increased the conversion rate of HMF, as the CuO present inhibited the side reactions. Increasing the ratio further (to 100%) slightly decreased the selectivity (to 93.8%), while the conversion rate continually increased. However, excessive catalyst use may result in a sharp decrease in

BHMF selectivity. This is likely due to a competition between the inhibitory effects of CuO on the catalyst surface and the promotional effects of BHMF concentration. Particularly, a higher BHMF concentration resulted in a higher reaction rate (nonzero-order). Therefore, an 80% catalyst/HMF ratio resulted in the optimal selectivity and was chosen for subsequent experiments.

A key modulating factor of the HMF hydrogenation reaction is the reaction time (Fig. 8). However, it is evident that increasing the reaction time from 4 to 5 h had a minimal effect on the HMF conversion rate, with the BHMF selectivity only slightly decreasing. This is because the catalyst exists in a state of equilibrium while the side reactions occur. This causes a leftward shift in equilibrium and a continuous conversion of BHMF to HEMF, although with a small conversion rate. To determine the activation energies of the primary and side reactions, a kinetic study was performed using suitable parameters based on the above results.

### 3.3 Kinetic modeling study

The aldehyde and hydroxyl groups (2,5 positions on the furan ring) react with ethanol in the presence of a suitable catalyst under specific temperature conditions. HMF is converted to BHMF and then undergoes etherification to produce HEMF (Scheme 1), with the selectivity dependent on reaction conditions. The hydrogenation process was performed at different temperatures (433, 443, and 453 K) to determine the kinetics parameters. In the CTH experiments, the hydrogen donor (10 mL) was used in excess compared to that of the substrate (1 mmol HMF) to ensure that a constant ethanol supply was available during the CTH process. Under these conditions, the kinetic rate constants and reaction activation energies were calculated using a pseudo-first-order model. The following set of derived ordinary differential equations was used to determine the kinetic parameters for the CTH of HMF [25,26]:

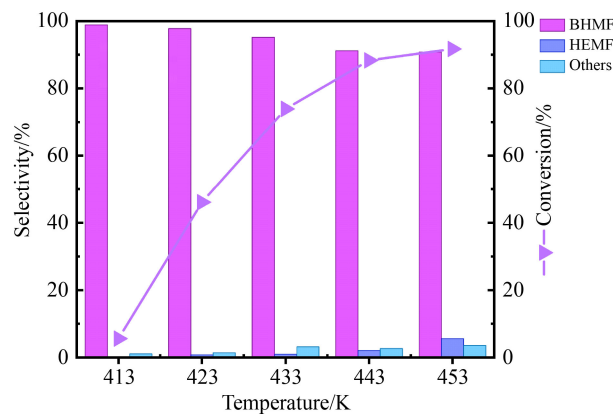


**Fig. 6** Effect of reaction temperature (reaction conditions: 10 mL ethanol, 1 mmol HMF, catalyst/HMF = 80%, time = 3 h).

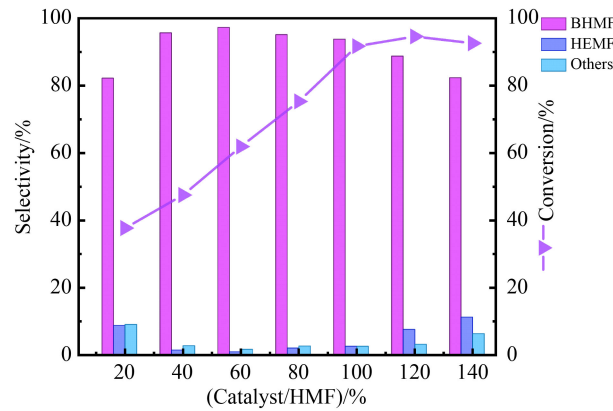


**Fig. 7** Effect of catalyst loading (reaction conditions: 10 mL ethanol, 1 mmol HMF, time = 3 h, temperature = 433 K).

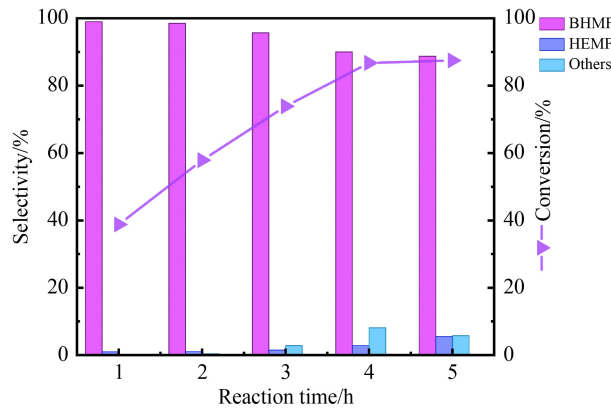
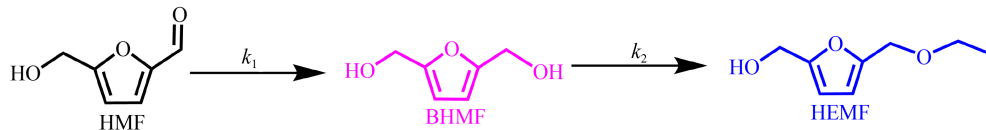


**Fig. 8** Effect of reaction time (reaction conditions: 10 mL ethanol, 1 mmol HMF, Catalyst/HMF = 80%, temperature = 433 K).



**Scheme 1** Reaction route for hydrogenation of HMF to BHMF.

$$\frac{d[HMF]}{dt} = -k_1 \times [HMF], \quad (1)$$

$$\frac{d[BHMF]}{dt} = k_1 \times [HMF] - k_2 \times [BHMF], \quad (2)$$

$$\frac{d[HEMF]}{dt} = k_2 \times [BHMF], \quad (3)$$

where  $k_1$  and  $k_2$  are the pseudo-first-order rate constants for the hydrogenation of HMF and etherification of BHMF at a specific reaction temperature, respectively, and  $t$  is the reaction time, h. The above equations can be integrated using the following initial conditions:  $t = 0$  and  $[HMF] = [HMF]_0$ . The concentrations and the reaction time can be expressed using the following equations:

$$[HMF] = [HMF]_0 \times \exp(-k_1 \times t), \quad (4)$$

$$[BHMF] = [\exp(-k_1 \times t) - \exp(-k_2 \times t)] \times [HMF]_0 \times \frac{k_1}{k_1 - k_2}, \quad (5)$$

$$[HEMF] = [k_1/(k_2 - k_1) \times \exp(-k_1 \times t) - k_2/(k_2 - k_1) \times \exp(-k_2 \times t)] \times [HMF]_0 + C. \quad (6)$$

Parameter C in Eq. (6) is a constant.

The parameters were estimated using OriginPro Learning Edition software by performing a nonlinear curve fit to the selected data with the corresponding rate

equation. Note that concentrations at equilibrium should not be used in the fitting program, and the kinetic model accounts for the reverse reaction process. Therefore, the rate equation fitting result derived from this model must contradict the concentrations at equilibrium. The experimental data curves fitted at the investigated reaction temperatures are shown in Fig. 9. Table 3 displays the activation energies as determined from the Arrhenius equation and the reaction rate constants corresponding to the investigated temperatures. The similarity between the experimental data and the fitted curves confirms that the pseudo-first-order reaction model accurately describes the CTH of HMF. The activation energy for BHMF formation ( $37.58 \text{ kJ}\cdot\text{mol}^{-1}$ ) is significantly lower than that of HEMF ( $86.89 \text{ kJ}\cdot\text{mol}^{-1}$ ) and also lower than recently reported activation energy value ( $60.83 \text{ kJ}\cdot\text{mol}^{-1}$ ) [27]. Thus, the kinetic study results explain the high BHMF selectivity.

### 3.4 Mechanism study

In the investigated reaction system, several hydroxyl and carbonyl groups reacted with each other through the MPV

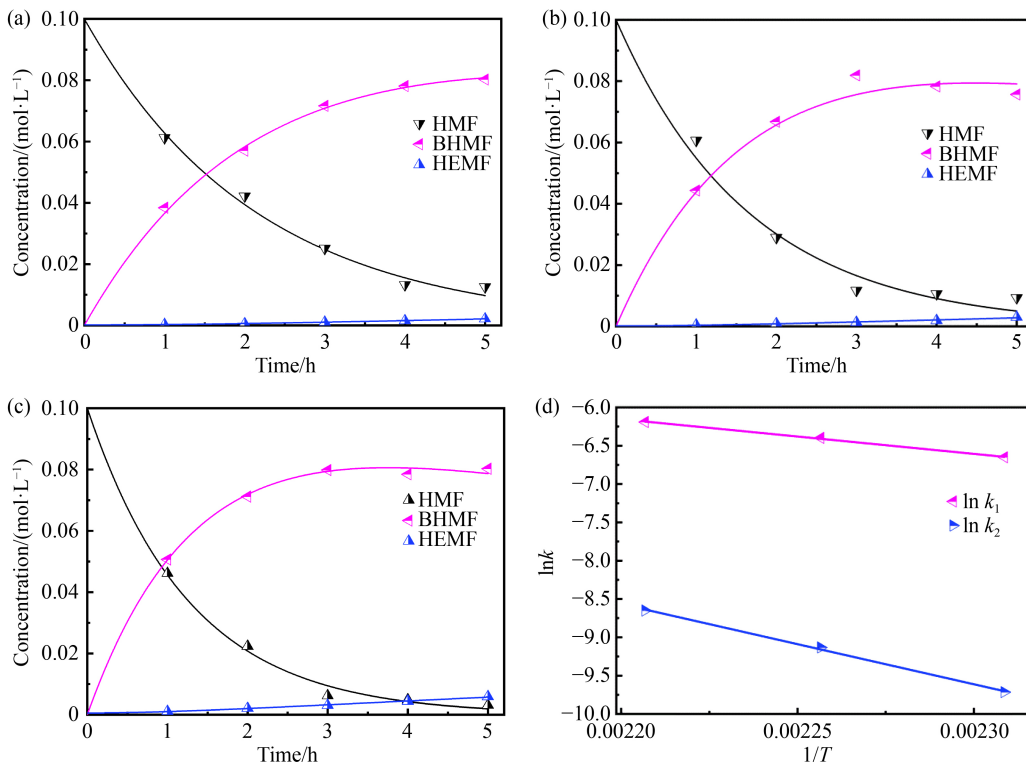


**Fig. 9** (a–c) Model (solid line) and experimental data (markers) of HMF, hydrogenation products (BHMF), and by-product (HEMF) over 40 wt % CuO/Bhm catalyst at 433, 443, and 453 K, and (d) Arrhenius plot.

**Table 3** Calculated kinetic parameters for the hydrogenation of HMF over the 40 wt % CuO/Bhm catalyst

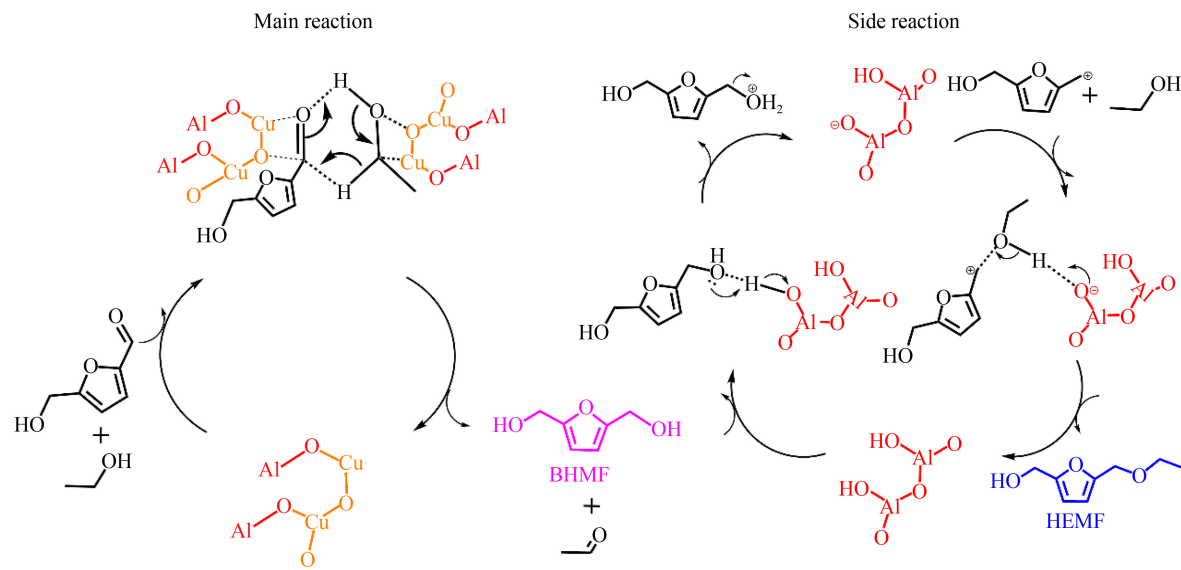
Rate constant	Reaction temperature/K			Activity energy/ (kJ·mol <sup>-1</sup> )	$R^2$
	433	443	453		
$k_1/\text{h}^{-1}$	0.46531	0.59920	0.73735	37.58	0.99615
$k_2/\text{h}^{-1}$	0.02172	0.04019	0.06297	86.89	0.99643

and etherification reactions. As previously discussed, CuO/Bhm contains Lewis acid sites ( $\text{Cu}^{2+}$ ), Brønsted acid sites ( $\text{H}^+$ ), and Lewis base sites ( $\text{O}^{2-}$ ), whose different roles determine the product distribution. The synergistic effects of the Lewis acid and base sites play a significant role in the MPV reduction of HMF to BHMF [28–31]. The Brønsted acid sites result in HEMF and etherification product formation. The BHMF selectivity can be significantly increased by increasing the Lewis acid/Brønsted acid ratio, which is achieved by modifying the Bhm surface with CuO. **Scheme 2** displays a plausible reaction mechanism for the selective hydrogenation of HMF to BHMF over the CuO/Bhm catalysts based on the experimental results. HMF and ethanol are initially adsorbed onto the catalyst surface via hydrogen-bonding interactions. Subsequently, the H and O atoms of the ethanol hydroxyl group are activated by interactions with the  $\text{O}^{2-}$  and  $\text{Cu}^{2+}$ , respectively, on the CuO/Bhm surface, facilitating the dissociation of the hydroxyl group in ethanol. Simultaneously, the O and C atoms of the HMF aldehyde group are also activated through interactions with the  $\text{Cu}^{2+}$  and  $\text{O}^{2-}$  ions. Finally, the activated ethanol and HMF form a six-membered-ring transitional intermediate with assistance from the  $\text{Cu}^{2+}$  and  $\text{O}^{2-}$  ions, resulting in the CTH and HMF reduction to BHMF. However, some Brønsted acid sites from the hydroxyl group remain on the catalyst surface, facilitating the reaction of BHMF with ethanol. Initially, the O atom of the hydroxyl group

in BHMF captures a proton to form an oxonium ion, generating a carbocation and an O anion on the CuO/Bhm surface. Subsequently, the H atom of the ethanol hydroxyl group is captured by the O anion on the catalyst surface. Meanwhile, the lone-pair electrons of the ethanol H–O bond are transferred to the carbocation, producing HEMF [32–34].

### 3.5 Recyclability of catalyst

The profiles of the catalyst reuse study are shown in **Fig. 10**. The reused catalyst sample was rinsed with 50 mL of ethanol before each use (**Fig. 10(a)**). The HMF conversion rate decreased from 89.3% to 28.5% over four usage cycles. A floating dark red colored powder was observed in the reaction solution. The catalyst was recovered by calcination at 673 K in air. **Figure 10(b)** shows the XRD patterns of the fresh and reused catalyst samples. The peaks related to Bhm (albeit slightly weakened) were also present in the XRD pattern of the reused sample, confirming the stability of the Bhm crystal structure. However, new diffraction peaks corresponding to the (111), (200), (220), and (311) lattice planes of Cu were observed at the  $2\theta$  of 43.2°, 50.4°, 74.1°, and 89.9°, respectively, which explain the presence of the dark red powder (Fig. S6, cf. ESM). Contrastingly, the CuO diffraction peaks were significantly weakened because the ethanol-reducing CuO reaction was carried out under high reaction temperature and pressurized conditions. Elemental Cu coated the catalytic active sites on the catalyst surface, leading to a decrease in the CuO/Bhm catalytic activity. The high-temperature treatment in air removed the metallic Cu coated on the catalyst surface, increasing the catalyst activity. The leaching test result indicated that the BHMF yield did not continuously increase, but slightly decreased. This is because of ether-



**Scheme 2** Mechanism of HMF hydrogenation over catalyst interfacial site.

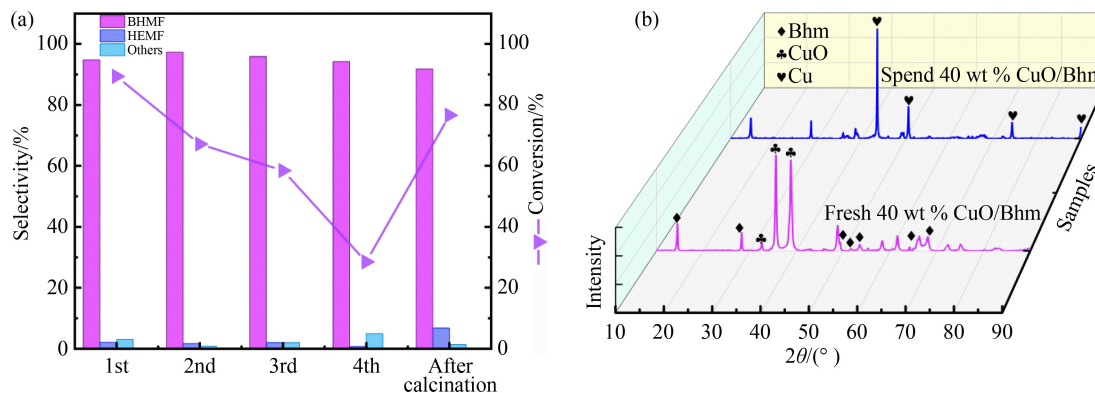


**Fig. 10** Profiles of the catalyst reuse study. (a) Catalyst recycling experiments (reaction conditions: 10 mL ethanol, 1 mmol HMF, catalyst/HMF = 100%, 433 K). (b) XRD patterns of the fresh and spent 40 wt % CuO/Bhm catalyst.

fication and other side reactions occurring after 40 wt % CuO/Bhm was removed by centrifugation over 1.5 h (Fig. S7, cf. ESM). This result demonstrated that the active sites were not leached and that the 40 wt % CuO/Bhm catalyst was heterogeneous. Therefore, metal agglomeration and partial CuO separation from the Bhm surface caused by the repeated calcination process may lead to incomplete catalytic performance recovery.

## 4 Conclusions

The selective transformation of HMF into BHMF was successfully performed over a non-noble metal catalyst (CuO/Bhm) using ethanol as both the solvent and hydrogen donor. It was observed that the target product selectivity depended on the difference between the main and side reaction rates, as well as their parallel or consecutive occurrence. Bhm contains both Lewis acid and base sites, which played a significant role in the CTH of HMF, while the hydroxyl group Brønsted acid ( $H^+$ ) on the Bhm surface catalyzed the etherification reaction. CuO addition reduced the side reaction rate, thereby improving the BHMF selectivity. The kinetic study results suggested that the rate constant for the transformation of HMF into BHMF is much larger than that of HEMF, the latter of which has an activation energy of  $86.89\text{ kJ}\cdot\text{mol}^{-1}$ , which is 2.3 times higher than for the conversion of HMF into BHMF. These results confirmed that the proposed method is suitable for the selective hydrogenation of HMF, contributing toward ongoing research efforts to exploit biomass energy.

**Acknowledgements** The authors gratefully acknowledge the financial support of the National Natural Science Foundation of China (Grant No. 22278121), Scientific Research Fund of Hunan Provincial Education Department (Grant No. 20B364), Hunan Provincial Innovation Foundation for Postgraduate (Grant No. QL20210132), and Science and Technology Planning Project of Hunan Province (Grant Nos. 2021GK5083, 2021GK4049, 2018TP1017).

**Electronic Supplementary Material** Supplementary material is available in the online version of this article at <https://dx.doi.org/10.1007/s11705-022-2225-4> and is accessible for authorized users.

## References

- Chen S, Wojcieszak R, Dumeignil F, Marceau E, Royer S. How catalysts and experimental conditions determine the selective hydroconversion of furfural and 5-hydroxymethylfurfural. *Chemical Reviews*, 2018, 118(22): 11023–11117
- Gerardy R, Debecker D P, Estager J, Luis P, Monbaliu J M. Continuous flow upgrading of selected C<sub>2</sub>–C<sub>6</sub> platform chemicals derived from biomass. *Chemical Reviews*, 2020, 120(15): 7219–7347
- Kucherov F A, Romashov L V, Galkin K I, Ananikov V P. Chemical transformations of biomass-derived C<sub>6</sub>-furanic platform chemicals for sustainable energy research, materials science, and synthetic building blocks. *ACS Sustainable Chemistry & Engineering*, 2018, 6(7): 8064–8092
- Hu L, Xu J, Zhou S, He S, Tang X, Lin L, Xu J, Zhao Y. Catalytic advances in the production and application of biomass-derived 2,5-dihydroxymethylfuran. *ACS Catalysis*, 2018, 8(4): 2959–2980
- Gilkey M J, Xu B. Heterogeneous catalytic transfer hydrogenation as an effective pathway in biomass upgrading. *ACS Catalysis*, 2016, 6(3): 1420–1436
- Rao K T V, Hu Y, Yuan Z, Zhang Y, Xu C C. Green synthesis of heterogeneous copper-alumina catalyst for selective hydrogenation of pure and biomass-derived 5-hydroxymethylfurfural to 2,5-bis(hydroxymethyl)furan. *Applied Catalysis A: General*, 2021, 609: 117892
- Arias K S, Carceller J M, Climent M J, Corma A, Iborra S. Chemoenzymatic synthesis of 5-hydroxymethylfurfural (HMF)-derived plasticizers by coupling HMF reduction with enzymatic esterification. *ChemSusChem*, 2020, 13(7): 1864–1875
- Zhao W, Huang Z, Yang L, Liu X, Xie H, Liu Z. Highly efficient syntheses of 2,5-bis(hydroxymethyl)furan and 2,5-dimethylfuran via the hydrogenation of biomass-derived 5-hydroxymethylfurfural over a nickel-cobalt bimetallic catalyst. *Applied Surface Science*, 2022, 577: 151968

9. Jing Y, Wang Y, Furukawa S, Xia J, Sun C, Hulsey M J, Wang H, Guo Y, Liu X, Yan N. Towards the circular economy: converting aromatic plastic waste back to arenes over a Ru/Nb<sub>2</sub>O<sub>5</sub> catalyst. *Angewandte Chemie International Edition*, 2021, 60(10): 5527–5535
10. Yang P, Xia Q, Liu X, Wang Y. Catalytic transfer hydrogenation/hydrogenolysis of 5-hydroxymethylfurfural to 2,5-dimethylfuran over Ni–Co/C catalyst. *Fuel*, 2017, 187: 159–166
11. Wang G H, Deng X, Gu D, Chen K, Tuysuz H, Spliethoff B, Bongard H J, Weidenthaler C, Schmidt W, Schuth F. Co<sub>3</sub>O<sub>4</sub> nanoparticles supported on mesoporous carbon for selective transfer hydrogenation of  $\alpha,\beta$ -unsaturated aldehydes. *Angewandte Chemie International Edition*, 2016, 55(37): 11101–11105
12. Hu L, Liu S, Song J, Jiang Y, He A, Xu J. Zirconium-containing organic–inorganic nanohybrid as a highly efficient catalyst for the selective synthesis of biomass-derived 2,5-dihydroxymethylfuran in isopropanol. *Waste and Biomass Valorization*, 2020, 11(7): 3485–3499
13. Chen N, Zhu Z, Su T, Liao W, Deng C, Ren W, Zhao Y, Lü H. Catalytic hydrogenolysis of hydroxymethylfurfural to highly selective 2,5-dimethylfuran over FeCoNi/h-BN catalyst. *Chemical Engineering Journal*, 2020, 381: 122755
14. Elsayed I, Jackson M A, Hassan E B. Hydrogen-free catalytic reduction of biomass-derived 5-hydroxymethylfurfural into 2,5-bis(hydroxymethyl)furan using copper–iron oxides bimetallic nanocatalyst. *ACS Sustainable Chemistry & Engineering*, 2020, 8(4): 1774–1785
15. Wang T, Zhang J, Xie W, Tang Y, Guo D, Ni Y. Catalytic transfer hydrogenation of biobased HMF to 2,5-bis(hydroxymethyl)furan over Ru/Co<sub>3</sub>O<sub>4</sub>. *Catalysts*, 2017, 7(3): 92
16. Zhang J, Qi Z, Liu Y, Wei J, Tang X, He L, Peng L. Selective hydrogenation of 5-hydroxymethylfurfural into 2,5-bis(hydroxymethyl)furan over a cheap carbon-nanosheets-supported Zr/Ca bimetallic catalyst. *Energy & Fuels*, 2020, 34(7): 8432–8439
17. Wang H, Liu B, Liu F, Wang Y, Lan X, Wang S, Ali B, Wang T. Transfer hydrogenation of cinnamaldehyde catalyzed by Al<sub>2</sub>O<sub>3</sub> using ethanol as a solvent and hydrogen donor. *ACS Sustainable Chemistry & Engineering*, 2020, 8(22): 8195–8205
18. Huang L, Zhu Y, Huo C, Zheng H, Feng G, Zhang C, Li Y. Mechanistic insight into the heterogeneous catalytic transfer hydrogenation over Cu/Al<sub>2</sub>O<sub>3</sub>: direct evidence for the assistant role of support. *Journal of Molecular Catalysis A: Chemical*, 2008, 288(1–2): 109–115
19. Kloprogge T J, Duong L V, Wood B J, Frost R L. XPS study of the major minerals in bauxite: gibbsite, bayerite and (pseudo-) boehmite. *Journal of Colloid and Interface Science*, 2006, 296(2): 572–576
20. Nazim M, Khan A A P, Asiri A M, Kim J H. Exploring rapid photocatalytic degradation of organic pollutants with porous CuO nanosheets: synthesis, dye removal, and kinetic studies at room temperature. *ACS Omega*, 2021, 6(4): 2601–2612
21. Majid A, Tunney J, Argue S, Kingston D, Post M, Margeson J, Gardner G J. Characterization of CuO phase in SnO<sub>2</sub>–CuO prepared by the modified Pechini method. *Journal of Sol–Gel Science and Technology*, 2010, 53(2): 390–398
22. Wang J, Zhang Z, Jin S, Shen X. Efficient conversion of carbohydrates into 5-hydroxymethylfuran and 5-ethoxymethylfuran over sulfonic acid-functionalized mesoporous carbon catalyst. *Fuel*, 2017, 192: 102–107
23. Li S, Dong M, Yang J, Cheng X, Shen X, Liu S, Wang Z Q, Gong X Q, Liu H, Han B. Selective hydrogenation of 5-(hydroxymethyl)furfural to 5-methylfurfural over single atomic metals anchored on Nb<sub>2</sub>O<sub>5</sub>. *Nature Communications*, 2021, 12(1): 584
24. Lu Y, Bradshaw J, Zhao Y, Kuester W, Kabotso D. Structure-reactivity relationship for alcohol oxidations via hydride transfer to a carbocationic oxidizing agent. *Journal of Physical Organic Chemistry*, 2011, 24(12): 1172–1178
25. Fachri B A, Abdilla R M, Bovenkamp H H, Rasrendra C B, Heeres H J. Experimental and kinetic modeling studies on the sulfuric acid catalyzed conversion of D-fructose to 5-hydroxymethylfurfural and levulinic acid in water. *ACS Sustainable Chemistry & Engineering*, 2015, 3(12): 3024–3034
26. Deng X, Zhao P, Zhou X, Bai L. Excellent sustained-release efficacy of herbicide quinclorac with cationic covalent organic frameworks. *Chemical Engineering Journal*, 2021, 405: 126979
27. He A, Hu L, Zhang Y, Jiang Y, Wang X, Xu J, Wu Z. High-efficiency catalytic transfer hydrogenation of biomass-based 5-hydroxymethylfurfural to 2,5-bis(hydroxymethyl)furan over a zirconium–carbon coordination catalyst. *ACS Sustainable Chemistry & Engineering*, 2021, 9(46): 15557–15570
28. Valekar A H, Lee M, Yoon J W, Kwak J, Hong D Y, Oh K R, Cha G Y, Kwon Y U, Jung J, Chang J S, Hwang Y K. Catalytic transfer hydrogenation of furfural to furfuryl alcohol under mild conditions over Zr-MOFs: exploring the role of metal node coordination and modification. *ACS Catalysis*, 2020, 10(6): 3720–3732
29. Vandichel M, Vermoortele F, Cottenie S, De Vos D E, Waroquier M, Van Speybroeck V. Insight in the activity and diastereoselectivity of various Lewis acid catalysts for the citronellal cyclization. *Journal of Catalysis*, 2013, 305: 118–129
30. Vermoortele F, Bueken B, Le Bars G, Van de Voorde B, Vandichel M, Houthoofd K, Vimont A, Daturi M, Waroquier M, Van Speybroeck V, Kirschhock C, De Vos D E. Synthesis modulation as a tool to increase the catalytic activity of metal–organic frameworks: the unique case of UiO-66(Zr). *Journal of the American Chemical Society*, 2013, 135(31): 11465–11468
31. Mironenko A, Vlachos G. Conjugation-driven “reverse Mars–Van Krevelen”-type radical mechanism for low-temperature C–O bond activation. *Journal of the American Chemical Society*, 2016, 138(26): 8104–8113
32. Erb B, Risto E, Wendling T, Goossen L J. Reductive etherification of fatty acids or esters with alcohols using molecular hydrogen. *ChemSusChem*, 2016, 9(12): 1442–1448
33. De S, Dutta S, Saha B. One-pot conversions of lignocellulosic and algal biomass into liquid fuels. *ChemSusChem*, 2012, 5(9): 1826–1833
34. Hu W, Wan Y, Zhu L, Cheng X, Wan S, Lin J, Wang Y. A strategy for the simultaneous synthesis of methyl alcohol and diethyl acetal with Sn- $\beta$ . *ChemSusChem*, 2017, 10(23): 4715–4724